APPLIED SCIENCES AND ENGINEERING

Microfluidic-derived montmorillonite composite microparticles for oral codelivery of probiotic biofilm and postbiotics

Zhonglin Fang, Xinyuan Yang, Luoran Shang*

Oral delivery of probiotics has shown promising effects in modulating the gut microbiota and treating ulcerative colitis (UC). However, the therapeutic efficacy is restricted by gastrointestinal assaults, poor mucosal adhesion, and single therapeutic modality. Here, we developed acid-resistant, gut-environment–responsive composite microparticles based on microfluidic electrospray for the oral codelivery of probiotic [*Lactobacillus acidophilus* (LA)] biofilm and postbiotics (indole-3-propionic acid). Montmorillonite was selected for supporting biofilm formation due to its cation-exchange capability and clearly defined biosafety. The montmorillonite-LA biofilm was effectively protected by the microparticles and markedly improved the intestinal retention. Upon oral administration, the composite microparticles notably alleviated colitis in mice, including reducing the inflammatory response, improving intestinal barrier function, and modulating the gut microbiota. Consequently, the composite microparticles show high potential for enhancing probiotic delivery efficacy and present a promising strategy for UC treatment.

INTRODUCTION

Oral delivery of probiotics represents a promising approach for treating ulcerative colitis (UC) by actively modulating host immunity, metabolism, and gut microbiota composition (*1*–*3*). However, hostile gastrointestinal (GI) environments (e.g., gastric acid, bile salts, and digestive enzymes) as well as inadequate mucosal adhesion result in low survival rates and short retention time for oral probiotics (*4*, *5*). Current strategies to counter these effects involve surface coating or chemical modification of probiotics to withstand harsh conditions and enhance their interactions with the mucosal layer of intestinal epithelial cells (*6*–*8*). Although elegant, the materials used for coating or modification may undergo complex chemical syntheses, which could potentially affect bacterial viability and in vivo safety. Further, a single therapeutic mode of probiotics may be insufficient to restore the disturbed flora owing to the complex and variable nature of gut microbiota and the diverse targets and mechanisms of UC (*9*, *10*). Therefore, a comprehensive platform with high biosafety and efficacy is required for oral probiotic delivery.

In this study, a microfluidic-derived montmorillonite-based composite delivery platform was proposed for UC treatment, as shown in Fig. 1. Montmorillonite is typically extracted from natural bentonite mines and is a commercially available over-the-counter drug with well-demonstrated safety. Montmorillonite can support bacteria biofilm formation because of its excellent cation-exchange capability. In acidic culture media, montmorillonite surface becomes positively charged by ion exchange and protonation, which is essential for enabling interactions with certain negatively charged probiotics to form biofilms (*11*). Although the formation of biofilms can enhance probiotic colonization, the ability of biofilms in withstanding the harsh environment when traversing through the GI tract during oral delivery is still limited. On the other hand, microfluidic technique has been well established in fabricating microparticles with tunable physicochemical properties specific to target environment features as drug delivery microcarriers (*12*, *13*). Moreover, by co-encapsulating multiple drugs or bioactive agents, synthetic therapeutic performances can be achieved. It is thus conceived that, by constructing pH-sensitive, intestinal-specific microparticles, montmorillonite-probiotic biofilms together with other auxiliary agents can be codelivered orally for UC treatment.

Here, we developed composite Ca-alginate (CA) microcarriers by microfluidic electrospray for codelivery of montmorillonite–*Lactobacillus acidophilus* (LA) biofilms (MLB) and indole-3-propionic acid (IPA) to enhance UC treatment. LA was chosen because of its ability to autonomously produce lactic acid during cultivation. CA exhibits excellent biocompatibility and pH responsiveness; it remains stable in the stomach and gradually swells and degrades in the neutral to slightly alkaline environment of the intestine, resulting in controlled release of the contents (*14*, *15*). IPA is a metabolic byproduct produced by gut microbiota that offers several therapeutic benefits. Postbiotics like IPA are bioactive compounds that can exert beneficial effects on the host's health, such as reducing inflammation, combating oxidative stress, and repairing the intestinal barrier. These effects help create a favorable colonization environment for codelivered probiotics (*16*, *17*). The experimental findings demonstrated more robust mucoadhesive capacity of MLB compared to LA. Furthermore, we confirmed that the MLB + IPA@CA microparticles effectively alleviate colonic inflammation, restore mucosal barrier function, and modulate the gut microbiota in a colitis mouse model. Therefore, the MLB + IPA@CA microparticles serve as highly effective platforms for oral probiotic delivery and UC treatment.

RESULTS

Preparation and characterization of MLB@CA microparticles

To induce MLB formation, sterile montmorillonite particles were cocultured with LA in the logarithmic growth phase for 48 hours. Montmorillonite that was not coincubated with LA was set as a control. Scanning electron microscopy (SEM) images showed no bacteria in the control group (Fig. 2A). In contrast, montmorillonite cocultured with LA displayed typical biofilms on its surface (Fig. 2B).

Shanghai Xuhui Central Hospital, Zhongshan-Xuhui Hospital, and the Shanghai Key Laboratory of Medical Epigenetics, the International Co-laboratory of Medical Epigenetics and Metabolism (Ministry of Science and Technology), Institutes of Biomedical Sciences, Fudan University, Shanghai 200032, China.
*Corresponding author. Email: luoranshang@fudan.edu.cn

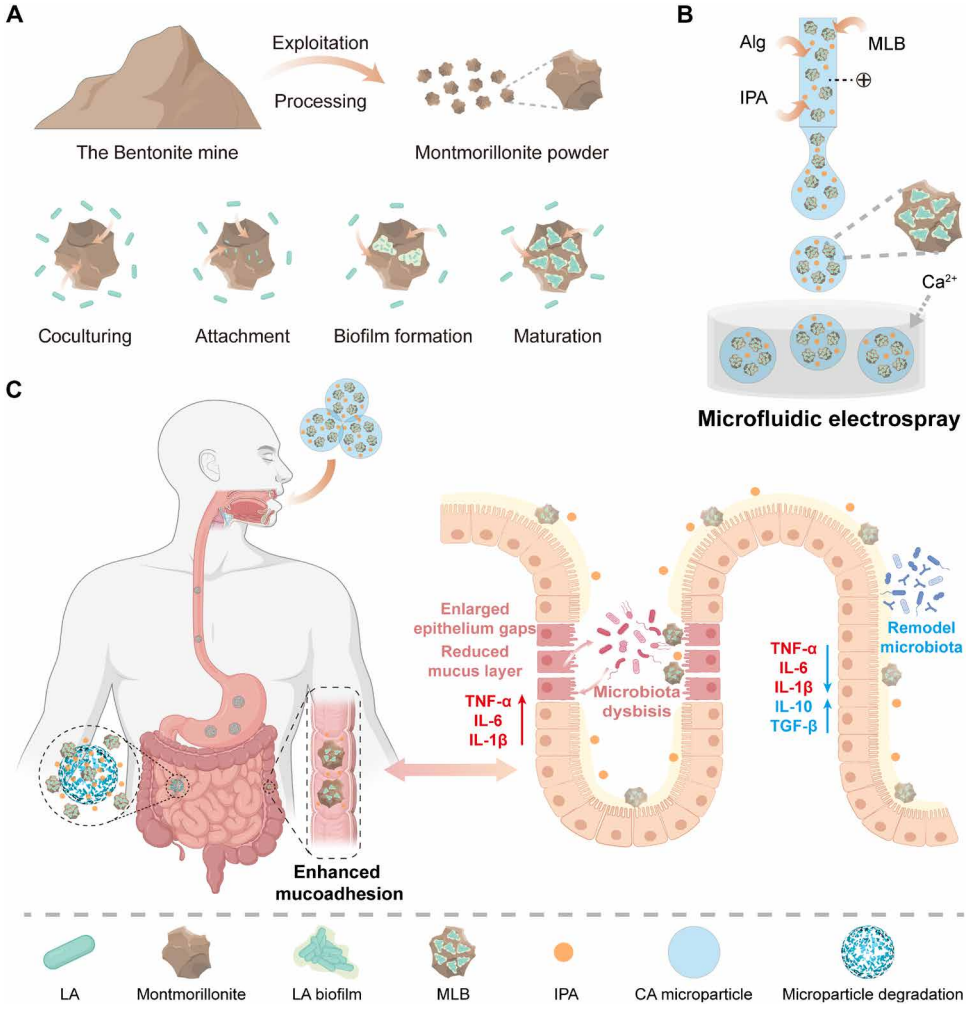

Fig. 1. Schematic diagram showing the microfluidic-derived montmorillonite composite microparticles for codelivery of probiotic biofilms and postbiotics for UC treatment. (**A**) Biofilm formation on montmorillonite. (**B**) Preparation of the montmorillonite composite microparticles by microfluidic electrospray. (**C**) Oral delivery of the montmorillonite composite microparticles and their therapeutic mechanism in treating UC. Graphic created with BioRender.com.

Concanavalin A tetramethylrhodame conjugate (ConA) staining was conducted to further verify the biofilm formation, as shown in Fig. 2C. Next, we determined whether montmorillonite switched its surface charge in an acidic culture medium. We measured the zeta potentials of montmorillonite under different pH conditions. The data indicated that montmorillonite was negatively charged under a neutral environment. However, it became positively charged at pH 5.1, and its positive charge further intensified at pH 4.2 (fig. S1). Alteration of the surface charge of montmorillonite initiates the adhesion of LA, which is crucial for the formation of MLB.

Next, MLB@CA microparticles were fabricated using microfluidic electrospray. In a typical experiment, the MLB was uniformly dispersed in an alginate solution and transferred into microfluidic channels, where droplets were formed under electrostatic forces and rapidly solidified in a collection bath containing 2.0% $CaCl_2$. Rapid cross-linking between Ca^{2+} and alginate effectively entrapped the MLB, resulting in the formation of MLB@CA microparticles. The size of the microparticles was precisely controlled by adjusting the flow rate and applied voltage. The data demonstrated that microparticle size increased with increasing flow rate and decreased with increasing voltage (fig. S2). We observed and statistically analyzed the morphology, size, and size distribution of MLB@CA at a voltage of 6 kV and a flow rate of 4 ml/hour. Under optical microscopy, the microparticles exhibited spherical integrity, uniform size, and excellent monodispersity (Fig. 2D), with particle sizes uniformly distributed around 300 μm (Fig. 2E). For comparison, CA microparticles without MLB were also fabricated at the same voltage and flow rate, and their arrangement and morphology were observed using optical microscopy and SEM (fig. S3). The surface morphology of MLB@CA was further characterized using SEM (Fig. 2F). In addition, the encapsulated MLB was clearly identified through the cross-sectional SEM observation of MLB@CA (fig. S4). Moreover, the prestained MLB was found to be uniformly distributed within the microparticles through two-dimensional (2D) and 3D confocal imaging (Fig. 2G and fig. S5).

The GI assault resistance and intestinal adhesiveness of MLB@CA

Invasion by the gastric acid and bile salts poses a challenge for the oral delivery of probiotics. As a pH-responsive drug delivery platform, the MLB@CA microparticles remained stable in stimulated gastric fluid

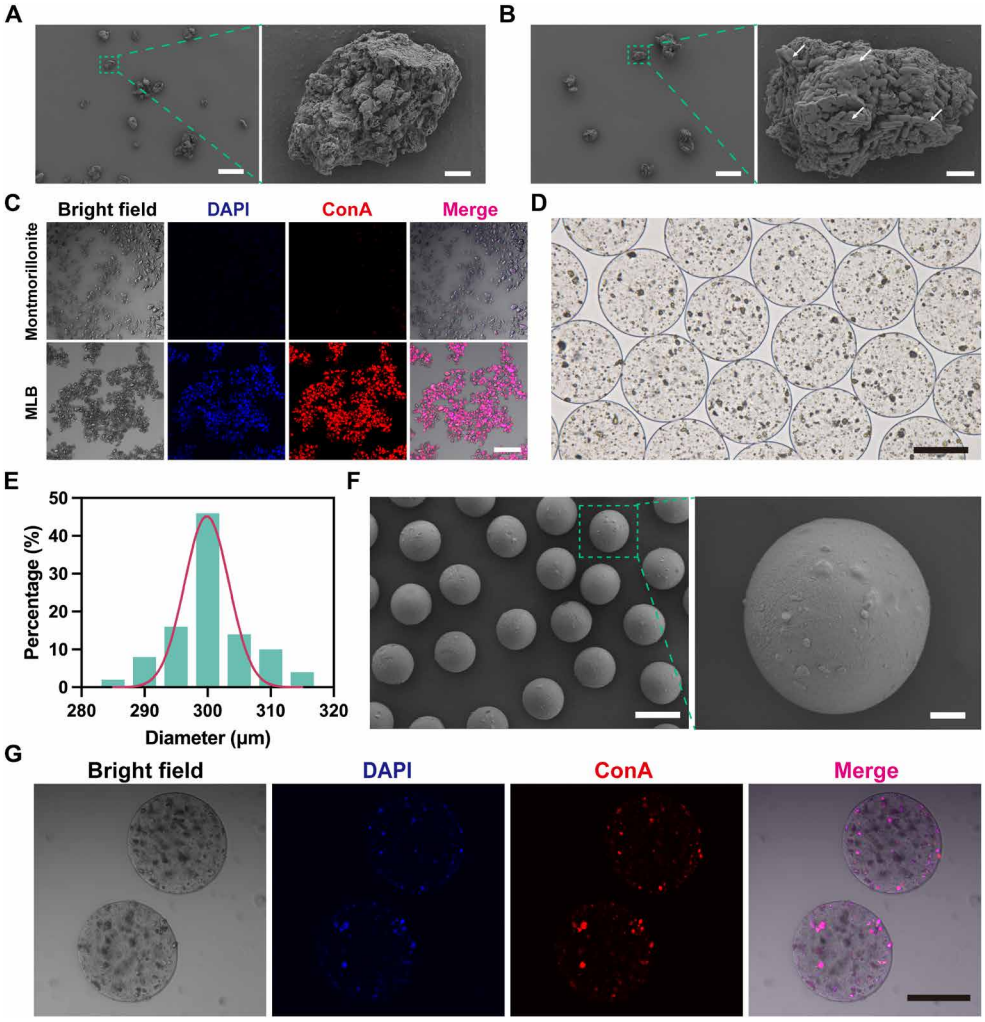

Fig. 2. Preparation and characterization of MLB and MLB@CA microparticles. (**A**, **B**, and **F**) SEM images of (A) montmorillonite, (B) MLB (white arrows indicate the LA biofilm), and (F) MLB@CA. (**C** and **G**) Confocal images of (C) MLB and (G) MLB@CA microparticles. The biofilm on montmorillonite was stained with 4′,6-diamidino-2-phenylindole (DAPI) and ConA. (**D** and **E**) (D) Optical image and (E) size distribution of MLB@CA microparticles. Scale bars, [(A) and (B)] 50 and 3 μm (magnified view), (C) 150 μm, [(D) and (G)] 200 μm, and (F) 300 and 50 μm (magnified view).

(SGF, pH 1.2) and gradually swelled and degraded in stimulated intestinal fluid (SIF, pH 6.8) (fig. S6). The protective effect of the microparticles was evaluated by testing the LA viability in SGF and SIF [with bile salt (0.3 mg/ml)]. After 4 hours of incubation in SGF, the bacterial survival rate in MLB@CA was 18.7%, whereas that in the MLB and LA groups showed almost complete loss of viability. Similarly, after 6 hours of incubation in SIF, the survival rate of LA in MLB@CA was 22.3%, which was significantly higher than that of MLB (10.3%) and LA (2.0%) groups (Fig. 3B). These results demonstrated that the CA microparticles effectively protected the viability of MLB. Furthermore, to assess the overall resistance within the GI tract, MLB@CA was evaluated for growth ability following sequential incubation in SGF (4 hours) and SIF (6 hours). The results showed that bacteria in the LA and MLB groups were unable to recover normal growth after incubation, whereas that in the MLB@CA group exhibited sustained growth in the culture medium (Fig. 3, C and D).

To investigate the mucosal adhesion of MLB, we evenly applied LA and MLB [both labeled with Cy5–*N*-hydroxysuccinimide (NHS) ester] to the mucosal layer of fresh porcine large intestine segments in vitro and incubated it for 1 hour. Fluorescence signals on the segments were visualized using an in vivo imaging system (IVIS) before and after phosphate-buffered saline (PBS) rinsing (Fig. 3E). Quantitative analysis indicated a significant reduction in the fluorescence intensity of LA after rinsing, whereas there was no noticeable change in the fluorescence intensity of MLB (Fig. 3F). Furthermore, in vivo adhesion of MLB was assessed by administering LA, MLB, and MLB@CA (all labeled with Cy5-NHS ester) to mice, followed by imaging the GI tract at predetermined time points. The IVIS images demonstrated higher fluorescence intensity and longer intestinal retention time in the MLB and MLB@CA groups (Fig. 3G). These results indicate that MLB exhibits stronger mucosal adhesion and prolonged intestinal retention than those of LA. We then quantified the *Lactobacillus* numbers in the stomach, small intestine, cecum, and colon at distinct time points following a single oral administration to comprehensively examine the adhesive properties of MLB and the protective effects of the MLB@CA microparticles. The data

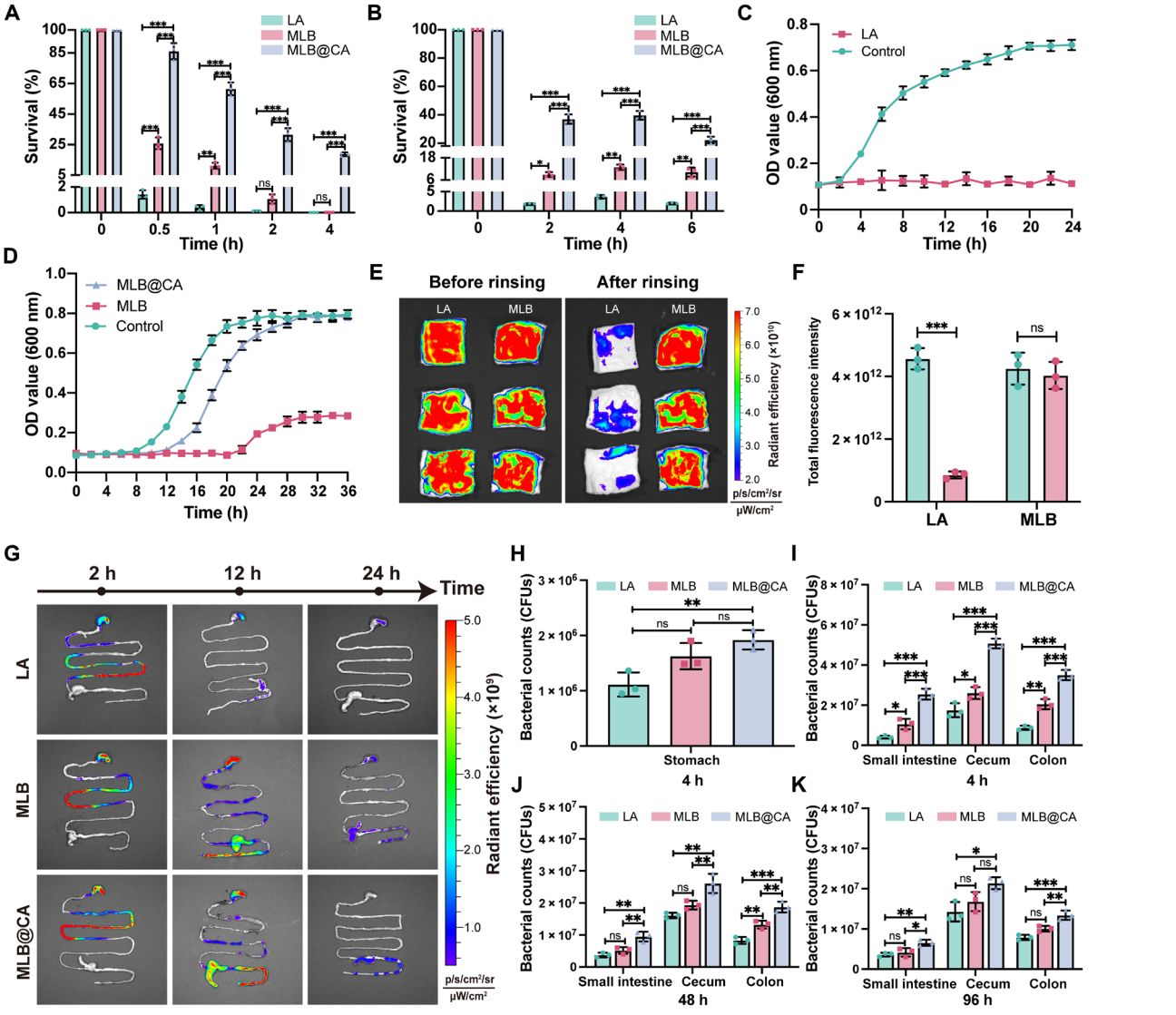

Fig. 3. Enhanced resistance of MLB@CA microparticles against GI environmental conditions and improved intestinal adhesion. (**A** and **B**) Bacterial viability in the LA, MLB, and MLB@CA groups after incubation in (A) SGF and (B) SIF. h, hours. (**C** and **D**) The growth curve of (C) LA, (D) MLB, and MLB@CA after 4-hour incubation in SGF and 6-hour incubation in SIF. "Control" represents unincubated (C) LA and (D) MLB. (**E**) IVIS images of porcine large intestine before and after rinsing. (**F**) Comparison of fluorescence intensity before and after rinsing. (**G**) Intestinal distribution in mice at distinct time points after oral administration of LA, MLB, and MLB@CA at equivalent amounts. (**H** to **K**) The amounts of *Lactobacillus* in different sites of GI tract at [(H) and (I)] 4, (J) 48, and (K) 96 hours after oral administration of an equivalent amount of LA, MLB, and MLB@CA. Data are presented as means ± SD ($n = 3$). *$P < 0.05$, **$P < 0.01$, ***$P < 0.001$.

revealed that the MLB@CA group had notably higher colony counts compared to the other groups at the corresponding time points (Fig. 3, H to K).

Encapsulation and release profile of IPA in MLB + IPA@CA

The above findings demonstrated the potential of orally delivered MLB@CA as a therapeutic strategy for UC. Next, we integrated postbiotic IPA into MLB@CA microparticles by co-encapsulating during the microfluidic fabrication process (fig. S7). We first plotted the standard curve of IPA based on known concentrations of IPA for subsequent analysis (fig. S8). We then systematically investigated the encapsulation efficiency (EE; %) and drug loading rate (DLR; %) of IPA in MLB + IPA@CA. As shown in Fig. 4A, increasing the initial IPA concentration from 0.5 to 2.0 mg/ml led to an increase in IPA loading from 1.03 to 3.55%, while maintaining the EE at approximately 80.0%. Considering the ease of dissolution, we selected 1.5 mg/ml of IPA as the initial concentration for subsequent use. Next, we studied the release kinetics of IPA. MLB + IPA@CA microparticles were exposed to SGF and SIF, respectively, to mimic IPA release in the GI tract. IPA showed slow release (<25.0%) within the first hour in SGF and achieving a cumulative release of (31.2 ± 1.59)% for over 10 hours. In contrast, a burst release (>50.0%) occurred in SIF within 1 hour, totaling (79.2 ± 2.54)% at 10 hours (Fig. 4B). We then aimed to determine whether the presence of IPA affects LA vitality. The growth and proliferation activity of LA were evaluated after co-incubation with IPA for 4 hours. Growth curves, Cell Counting Kit–8

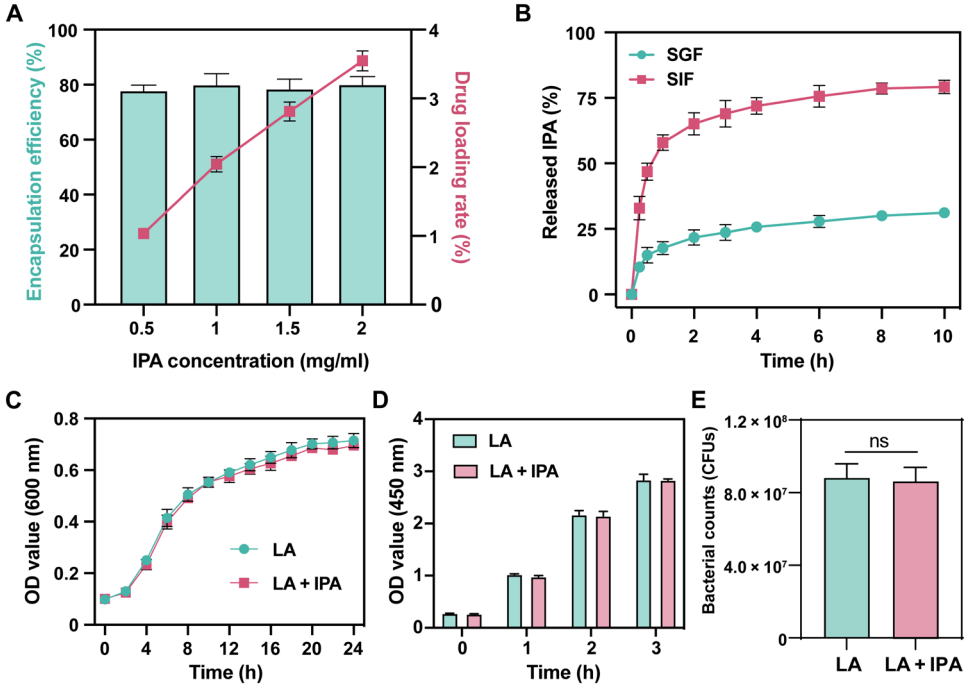

Fig. 4. Loading and release properties of IPA and the effect of IPA on LA viability. (**A**) The EE and DLR of IPA in MLB + IPA@CA microparticles with different initial IPA concentrations. (**B**) Release profile of IPA in SGF and SIF. (**C** to **E**) (C) The growth curve, (D) cell proliferation tested by CCK-8, and (E) colony counts of LA and LA + IPA after incubating for 4 hours. Data are presented as means ± SD ($n = 3$). h, hours.

(CCK-8) assays, and colony counting results indicated that IPA did not significantly affect the vitality of LA (Fig. 4, C to E, and fig. S9). We also investigated whether montmorillonite adsorbs IPA, potentially reducing the free IPA concentration. Analysis of the supernatant absorbance following montmorillonite and IPA coincubation revealed no significant decrease in IPA concentration, indicating that the influence of montmorillonite on IPA concentration could be considered negligible (fig. S10).

In vitro and in vivo safety assessment

Before verifying the in vivo safety, we first assessed the material's safety at the cellular level. NIH 3T3 cells were exposed to the leachate of montmorillonite + IPA@CA microparticles for 1 to 3 days. As shown in fig. S11A, the cells maintained normal morphology and exhibited healthy growth, indicating the microparticles' low toxicity. The CCK-8 assay further confirmed the normal proliferation of cells, with no significant differences observed compared to the control group (fig. S11B). To assess the biocompatibility of MLB + IPA@CA, the microparticles were dispersed in a 1.0% carboxymethyl cellulose (CMC) solution and orally administered to mice for 5 days (Fig. 5A). CMC demonstrates excellent biocompatibility and biodegradability (*18*, *19*). The microparticles in the CMC solution can maintain their structural integrity. Moreover, CMC facilitates the suspension of the microparticles, thereby allowing for controlled dosing. Five days after administration, blood and vital organs were collected. Hematological analysis showed that mice treated with MLB + IPA@CA had routine blood indices similar to those of healthy mice, as confirmed by typical indices such as white blood cells, red blood cells, hemoglobin, mean corpuscular volume, and platelets (Fig. 5B). We also evaluated various indicators based on serum samples. Biochemical tests revealed no notable differences in the indicators of liver and kidney function between mice treated with MLB + IPA@CA and CMC, confirming the absence of hepatorenal toxicity (fig. S12, B and C). In addition, no significant reduction in body weight or colon length was observed after treatment with MLB + IPA@CA (Fig. 5C and fig. S12A). Hematoxylin and eosin (H&E) staining of vital organs and tissues revealed normal morphology and structure in mice treated with MLB + IPA@CA (Fig. 5D). These results indicate that MLB + IPA@CA exhibits excellent biocompatibility.

Therapeutic role of MLB + IPA@CA in treating colitis

Next, we assessed the in vivo therapeutic effects of MLB + IPA@CA in mice with dextran sulfate sodium (DSS)–induced colitis. The mice were administered with CA, LA, MLB, MLB@CA, and MLB + IPA@CA via oral gavage for five consecutive days, and samples of feces, blood, and colon were obtained on day 12 for further examination, as depicted in Fig. 6A. Throughout the modeling and dosing periods, we monitored the daily changes in mouse body weight and evaluated the disease activity index (DAI). Our data revealed that mice treated with CMC consistently lost weight and exhibited increased DAI scores without any signs of improvement. In contrast, the MLB + IPA@CA group exhibited the most significant recovery (Fig. 6, B and C). Furthermore, mice treated with CMC exhibited colon lengths approximately half of those in the healthy mice. The other treatment groups displayed varying degrees of recovery, with the MLB + IPA@CA group showing significantly greater colon length, approaching that of healthy mice (Fig. 6, D and E). The levels of tissue damage and inflammation in the colon were examined by H&E staining. The results showed that the colonic epithelium was severely damaged in the CMC-treated group, which was characterized by the loss of crypt-like structures and extensive infiltration of lymphocytes and neutrophils. In contrast, MLB + IPA@CA effectively reversed pathological injury

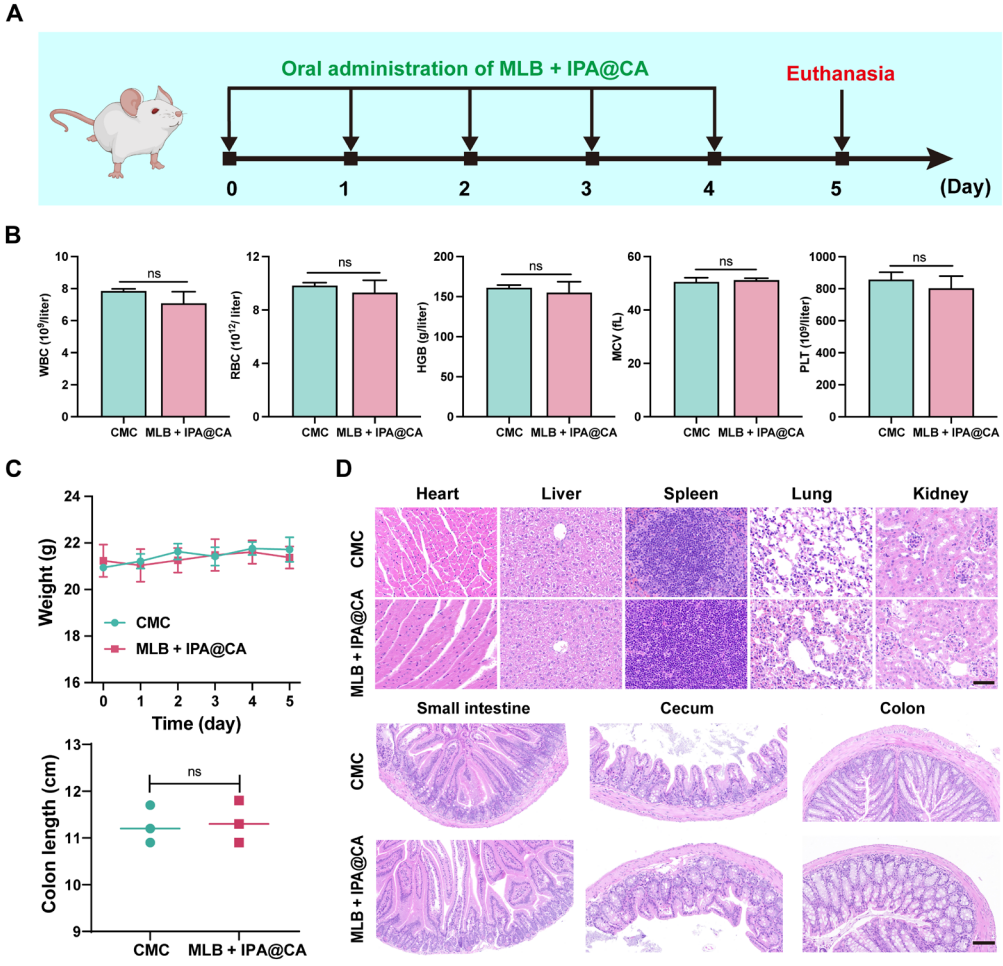

Fig. 5. Biocompatibility of MLB + IPA@CA microparticles in mice. (**A**) Schemes of the experimental procedures. (**B**) Typical blood routine indices. (**C**) Weight changes during administration and colon length measured after dissection. (**D**) H&E staining images of representative organs and tissues. Scale bars, 50 and 100 μm. Data are presented as means ± SD ($n = 3$).

of the colon (Fig. 6F). Collectively, these results indicate the superiority of MLB + IPA@CA over the other treatments, highlighting the comprehensive performance of MLB + IPA@CA and the synergistic effects of MLB and IPA.

Considering the excellent therapeutic efficacy of MLB + IPA@CA, we next aimed to elucidate its anti-colitis effects. First, serum concentrations of inflammatory cytokines were quantified through enzyme-linked immunosorbent assay (ELISA). Compared to the CMC treatment group, the MLB + IPA@CA treatment group showed significant reductions in proinflammatory cytokines such as tumor necrosis factor–α, interleukin-6 (IL-6), and IL-1β, while anti-inflammatory cytokines such as IL-10 and transforming growth factor–β were markedly increased (Fig. 7A). We also examined the expression level of myeloperoxidase (MPO) in colon using immunohistochemistry. MPO is a common glycoprotein primarily secreted by neutrophils and reflects the degree of inflammatory cell infiltration in tissues (*20*). Our findings indicated that MLB + IPA@CA effectively reduced the expression of MPO (fig. S13). Furthermore, we conducted terminal deoxynucleotidyl transferase–mediated deoxyuridine triphosphate nick end labeling staining of colon tissues to estimate the apoptosis levels in colonic epithelial cells. As shown in fig. S14, the CMC-treated group demonstrated substantial apoptosis of colonic epithelial cells, whereas the MLB + IPA@CA treatment group showed the lowest number of apoptotic cells.

UC is also characterized by the deterioration of intestinal mucosal and physical barrier functions (*21*). Next, we explored the effects of MLB + IPA@CA on intestinal barrier function. Alcian blue–periodate acid Schiff (AB-PAS) staining indicated that MLB + IPA@CA treatment effectively restored the mucous layer, whereas the mucus exhibited different degrees of disruption or irregular distribution in other groups of DSS-treated mice (Fig. 7B). In addition, we examined the expression of the intestinal epithelial tight junction proteins ZO-1 and Occludin-1, which are essential components of the intestinal physical barrier. The immunofluorescence images demonstrated that the expression levels of both proteins in the CMC-treated group were significantly down-regulated yet effectively reversed by the MLB + IPA@CA treatment (Fig. 7C).

Modulation of the gut microbiota in colitis mice

Increasing evidence suggests that UC development is closely associated with changes in gut microbiota, such as reduced microbial diversity, a decline in beneficial bacteria, and functional disruptions (*22*). Therefore, we examined whether MLB + IPA@CA treatment could effectively modulate the gut microbiota. Fecal samples collected on

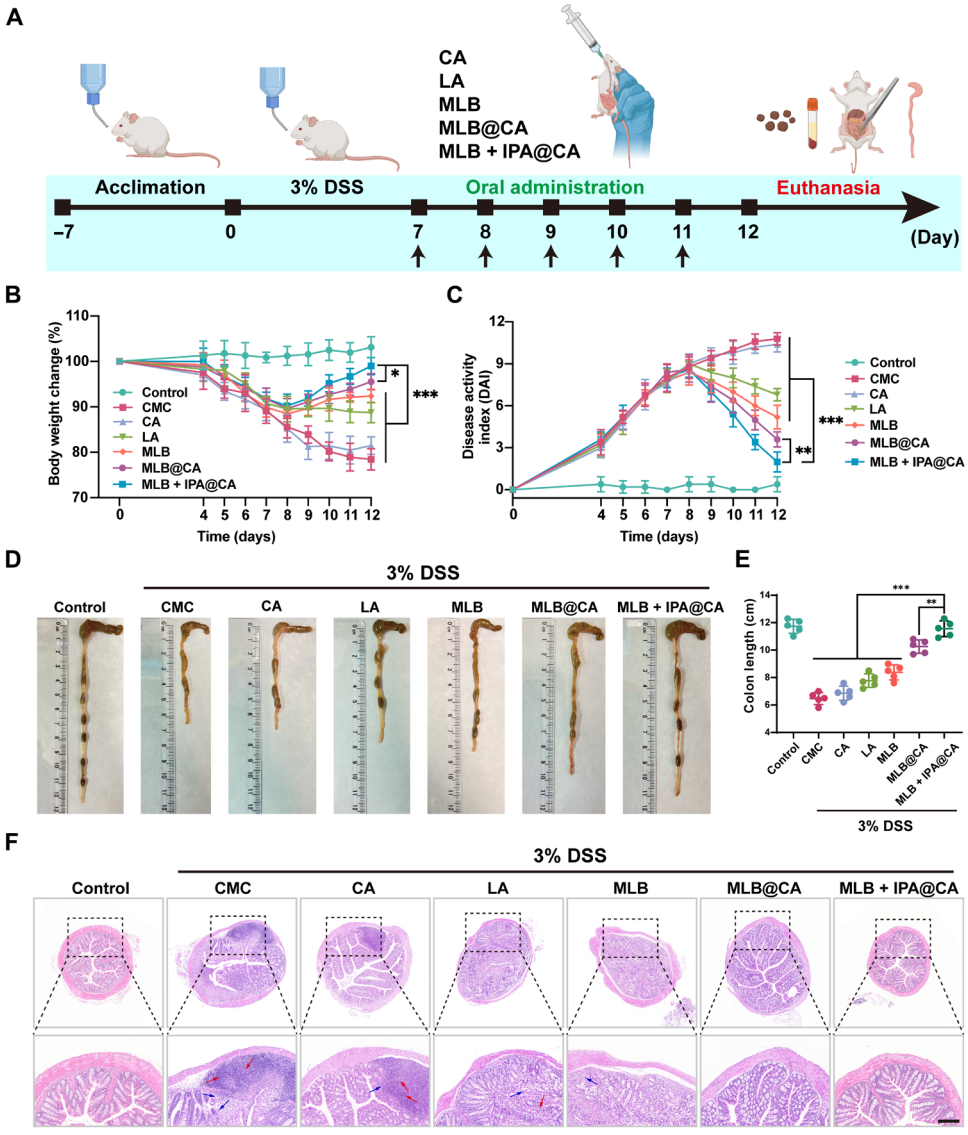

Fig. 6. Enhanced in vivo therapeutic effects of MLB + IPA@CA against DSS-induced colitis. (**A**) Schemes of experimental procedures, including colitis modeling, oral gavage, and dissection. (**B** and **C**) Curves of (B) body weight change and (C) DAI scores of mice during colitis modeling and oral administration. (**D**) Typical colon images of mice. (**E**) Colon lengths of mice. (**F**) Typical H&E staining images of colon tissues (red arrows indicate lymphocyte infiltration, and blue arrows indicate neutrophil infiltration). Scale bars, 200 μm. Data are presented as means ± SD ($n = 5$). *$P < 0.05$, **$P < 0.01$, ***$P < 0.001$.

day 12 were analyzed by 16*S* ribosomal DNA (rDNA) sequencing. We assessed the community richness and evenness of gut microbiota by analyzing α-diversity indices including the Chao1, Shannon, and Inverse-Simpson. The data revealed a significant decrease in the gut microbiota richness and diversity in CMC-treated mice. Conversely, the α-diversity indices were effectively restored after treatment with MLB + IPA@CA (Fig. 8, A to C). β-Diversity analysis using UniFrac distance–based principal coordinates analysis indicated that the microbiota profile of MLB + IPA@CA–treated mice was the most similar to that of healthy mice (Fig. 8D).

Subsequently, we examined the gut microbiota abundance at different taxonomic levels. The relative abundances of the top 10 microbiota at the phylum level were calculated and shown in Fig. 8E. In general, an increased ratio of *Bacteroidetes* to *Firmicutes* reflects gut microbiota dysbiosis. Statistical analysis showed that the MLB + IPA@CA treatment effectively reduced the ratio of *Bacteroidetes* to *Firmicutes* (Fig. 8F). Furthermore, we investigated the relative abundances of the top 10 gut microbiota at the family level and conducted the corresponding statistical analyses (Fig. 8G and fig. S15). The data indicated that treatment with MLB + IPA@CA markedly enhanced the relative abundance of *Muribaculaceae*, *Lachnospiraceae*, *Lactobacillaceae*, and *Prevotellaceae* while reducing that of *Bacteroidaceae* and *Tannerellaceae*. Previous studies have shown that *Muribaculaceae* and *Prevotellaceae* exhibit protective effects against colitis (*23*, *24*), while *Bacteroidaceae* is positively associated with colitis (*25*, *26*). *Lachnospiraceae* are capable of generating short-chain fatty acids, inhibiting the proliferation of pathogenic bacteria, and modulating the host immune response (*27*). At the genus level, the relative abundances of *Lactobacillus*, *Roseburia*, and *Bifidobacterium* were significantly increased after treatment with MLB + IPA@CA (Fig. 8H

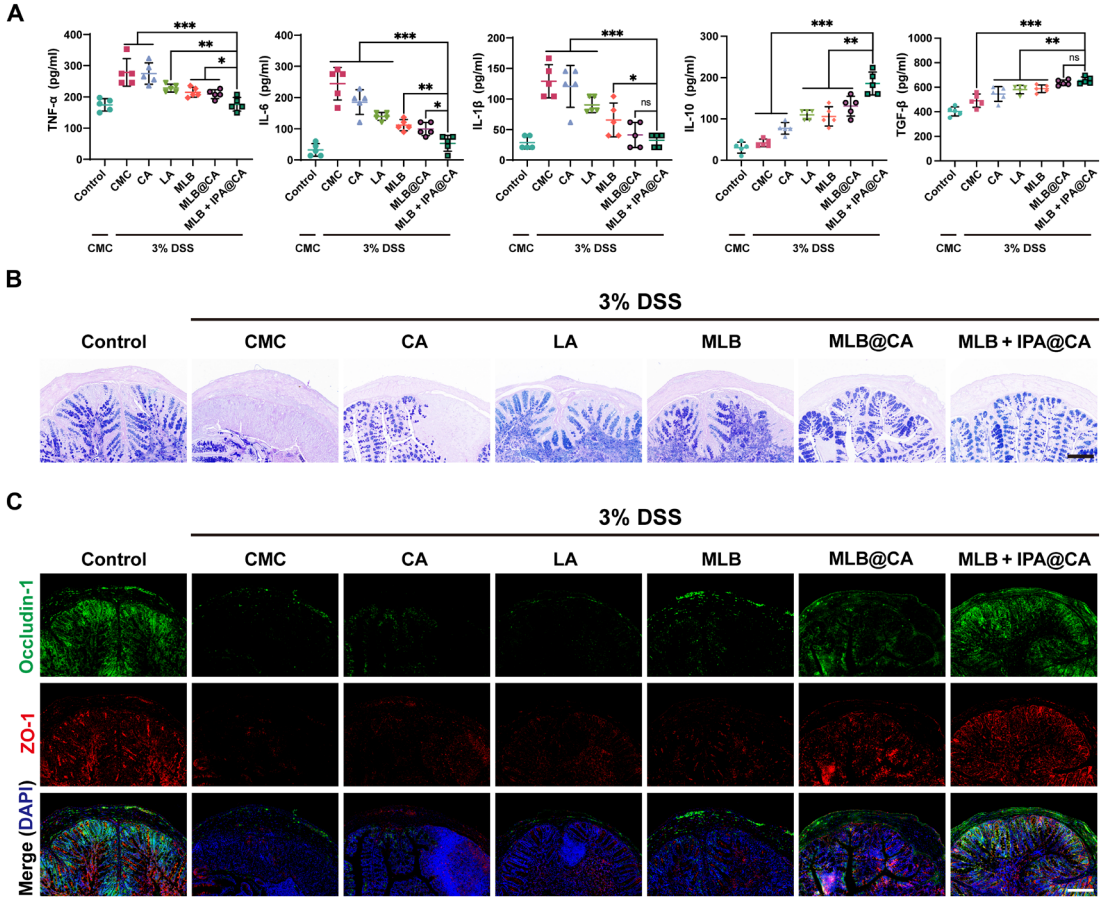

Fig. 7. Inflammatory inhibition and intestinal barrier repair effects of MLB + IPA@CA. (**A**) The levels of inflammatory cytokines in serum samples, measured using ELISA. (**B**) Typical images of AB-PAS staining of the colon. (**C**) Typical immunofluorescence staining images of tight junction proteins. Scale bars, (B and C) 200 μm. Data are presented as means ± SD ($n = 5$). *$P < 0.05$, **$P < 0.01$, ***$P < 0.001$.

and fig. S16). *Roseburia* produces butyrate, which is essential for maintaining the intestinal barrier integrity and preventing the proliferation and translocation of intestinal pathogens (*28*). *Bifidobacterium* is renowned for its ability to enhance the expression of epithelial tight junction proteins and protect the mucosal barrier (*29*). In addition, functional predictions based on Tax4Fun were used to further analyze the alterations in functional genes (Fig. 8I). The results showed that MLB + IPA@CA treatment effectively reversed the microbial functional changes induced by DSS, making them most similar to those observed in healthy mice. More specifically, MLB + IPA@CA treatment decreased the microbiota associated with infection and cancer development. A *t* test between the CMC and MLB + IPA@CA groups further demonstrated significant differences in the microbiota associated with disease infection, cancer development, and other functions (fig. S17). Together, these results suggest that MLB + IPA@CA can significantly alleviate the microbiota disturbance caused by DSS-induced colitis and bring it close to the level of healthy mice.

DISCUSSION

In this research, we developed montmorillonite composite microparticles based on microfluidics for efficient delivery of probiotic biofilms and postbiotics. These microparticles assist in overcoming GI assaults and respond to intestinal conditions for controlled release. Montmorillonite was used to support MLB formation owing to its natural source, biosafety, and excellent ion-exchange capacity. MLB greatly enhanced intestinal adhesion, thereby prolonging probiotic retention. In addition, microfluidic-generated microparticles act as codelivery vehicles, facilitating facile integration of IPA and thus synergizing with MLB to combat colitis. Our study demonstrated that the oral delivery of MLB + IPA@CA composite microparticles safely and effectively alleviated colitis, as well as reshaped the gut microbiota in mice.

The effective oral delivery of probiotics hinges on protecting their viability and optimizing their retention time within the GI tract. In recent years, various surface modification strategies, e.g., the use of lipid membranes, mucin, and polyphenols, have been extensively investigated to enhance probiotic delivery (*4*, *29*, *30*). However, whether chemical modification of probiotics will compromise the functionality and restrict the expansion of live microorganisms still needs further investigation.

To avoid this challenge, we leveraged the ion-exchange properties of montmorillonite under acidic conditions, which facilitates the spontaneous formation of probiotic biofilms on its surface. These biofilms consist of a 3D matrix of bacteria and extracellular polymeric

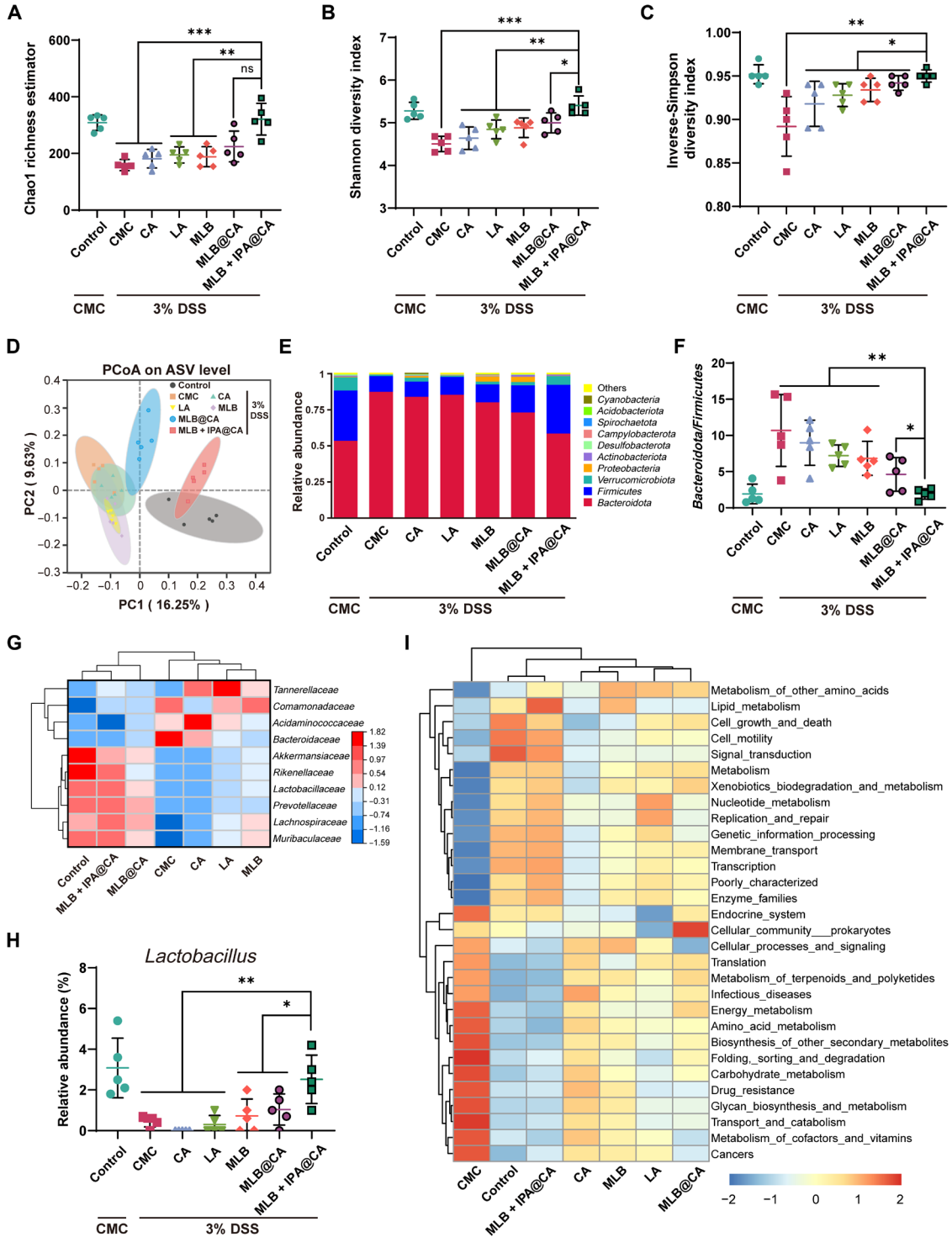

Fig. 8. Modulation of gut microbiota by oral delivery of MLB + IPA@CA. (**A** to **C**) Three α-diversity indices of gut microbes. (**D**) Principal coordinates analysis showing the β-diversity of gut microbes. (**E**) Relative abundance of the 10 most prevalent phyla among gut microbes. (**F**) Proportion statistics of *Bacteroidetes* and *Firmicutes*. (**G**) Cluster heatmap of the 10 most gut microbes categorized at the family-level taxonomy. (**H**) Relative abundance of *Lactobacillus*, categorized at the genus-level taxonomy. (**I**) Cluster heat map of predicted microbial function based on Tax4fun, highlighting the top 30 functional genes in gut microbes. Data are presented as means ± SD (n = 5). **P* < 0.05, ***P* < 0.01, ****P* < 0.001.

substance (EPS), conferring enhanced stability. Furthermore, exopolysaccharides and bacterial surface proteins integral to the biofilm structure affect the probiotic's ability to adhere to intestinal tissues (*31*).

To further optimize the biofilm's stability under gastric conditions and enable controlled release in response to intestinal stimuli, we used a microfluidic-based microencapsulation technology. By fine-tuning flow rates and voltage parameters, we were able to achieve precise control over droplet size, ensuring minimal variability in the produced microparticles. This system also offers the flexibility to incorporate additional bioactive molecules, such as postbiotics, which can act synergistically to enhance the therapeutic efficacy. Given the mild preparation conditions and the safety of the materials used, our microparticle delivery system has demonstrated favorable safety profiles in both cellular level and murine models. In vivo studies further corroborate that the microparticles effectively alleviate colitis symptoms in mice, restore intestinal barrier function, and positively modulate the gut microbiome.

While montmorillonite may alleviate colitis-induced diarrhea, it is not intended as a primary treatment for colitis. However, its therapeutic potential can be significantly enhanced when combined with probiotics. Furthermore, the composite microparticles hold promise for broader therapeutic applications beyond UC. Conditions such as metabolic syndrome, obesity, and autoimmune diseases linked to gut dysbiosis could potentially benefit from this delivery system. By tailoring the formulation to include specific bioactive compounds targeting the unique microbial imbalances associated with these disorders, condition-specific therapeutic strategies can be developed.

Given the versatility of the microfluidic encapsulation technology, we expect that more types of natural derived materials supporting probiotic biofilm formation can be developed. In addition, future studies should focus on improving the long-term stability of the formulation and ensuring that the probiotic viability is well preserved during storage.

MATERIALS AND METHODS

Materials

Montmorillonite was purchased from Simcere. IPA, calcium chloride ($CaCl_2$), sodium alginate (Na-Alg), and sodium citrate were purchased from Aladdin. CMC was purchased from Macklin. *L. acidophilus* ATCC4356 was obtained from Biobw. De Man-Rogosa-Sharpe (MRS) broth/agar and *Lactobacillus* selective agar were purchased from Hope Bio. DAPI (4′,6-diamidino-2-phenylindole) was purchased from Beyotime Biotechnology. Con A was purchased from Thermo Fisher Scientific. Cy5-NHS ester was obtained from Duofluor Inc. DSS was purchased from Meilunbio.

Animals

All animal experiments were carried out following the Guidelines for the Care and Use of Laboratory Animals of Fudan University and approved by the Animal Ethics Committee of Fudan University (approval no. 202405FD0005). BALB/c mice (female, 8 weeks old) were provided by Shanghai Lingchang Biotechnology Co. Ltd. (SCXK 2023-0003) and kept in specific pathogen-free environments.

Preparation and characterization of MLB

Montmorillonite was sieved through 400-mesh and 1000-mesh screens to obtain particles of 10 to 30 μm, followed by ultraviolet irradiation for 1 hour for sterilization. LA was anaerobically cultured in MRS liquid medium for 10 hours until reaching an optical density at 600 nm (OD_{600}) of 0.5. Subsequently, sterilized montmorillonite was added to the medium and further cultured for 48 hours. MLB samples were isolated from the culture medium by centrifugation (1000 rpm, 2 min), subsequently washed with PBS, freeze-dried, and examined by SEM (ZEISS Sigma 300) under high vacuum environment. In addition, fluorescent staining of biofilm was performed. The MLB samples were deposited onto glass slides and dried in a 37°C incubator. Subsequently, the samples were immersed in a 2.5% glutaraldehyde solution and fixed for 1 hour. The staining process involved incubation with ConA (555/580 nm) for 1 hour, followed by incubation with DAPI (340/488 nm) for 20 min. Last, the slides were sealed and imaged using confocal microscope (Leica SP8).

Count of bacteria on the montmorillonite

A certain amount of MLB was dispersed in sterile PBS. The bacteria within the biofilm were extracted via low-power ultrasonication, and the bacterial count of MLB was roughly calculated by spreading onto the MRS agar plate and cultured for 48 hours for colony counting.

Preparation and characterization of MLB@CA microparticles

The microfluidic device for generating microparticles included a glass capillary (outlet diameter: 180 μm) immobilized in a glass slide. MLB [1.0×10^8 colony-forming units (CFUs)] was uniformly dispersed in a Na-Alg solution (1.5%, w/v). All solutions were injected into the microfluidic channels via syringes. The microfluidic capillary was positioned 8.0 cm above a collection reservoir and subjected to a high static voltage (4 to 8 kV) to produce droplets. The collection reservoir contains a $CaCl_2$ solution (2.0%, w/v), where droplets rapidly cross-linked into microparticles in the presence of Ca^{2+}. The morphologies of MLB@CA microparticles were examined via optical microscopy, accompanied by particle size measurement. After the microparticles underwent CO_2 critical point drying, they were cut to reveal their cross sections, which were then examined by SEM. In addition, MLB@CA microparticles were observed by confocal laser scanning microscope (CLSM), and the MLB was prestained with DAPI and ConA.

Resistance assessments in vitro

MLB@CA, MLB, and LA (1.0×10^8 CFUs) were resuspended in 2 ml of SGF [(pH 1.2) 0.2 g NaCl and 0.32 g of pepsin per 1000 ml of ddH_2O] and 2 ml of SIF [(pH 6.8) with bile salts (0.3 mg/ml)]. At designated intervals, MLB and LA suspensions were centrifugated, resuspended, and plated onto MRS agar for colony counting. To assess the viability of LA after GI transit, MLB@CA, MLB, and LA (1.0×10^8 CFUs) were subjected to a 4-hour incubation in SGF and subsequently a 6-hour incubation in SIF. The suspensions were then transferred to MRS liquid medium, and the OD_{600} value was recorded every 2 hours to plot a growth curve. For MLB@CA microparticles, degradation in a sodium citrate solution (0.06 M) was required before the released MLB could be dispersed into MRS solid or liquid medium.

In vitro adhesion experiment

Fresh segments of porcine large intestines were uniformly cut to expose the mucosal layer. Both LA and MLB were labeled with Cy5-NHS ester and evenly applied onto the intestinal segments, followed by a 30-min incubation at 37°C with gentle rotation at 30 rpm. After that, the intestinal segments were imaged using an IVIS, and fluorescence signals were recorded. Subsequently, the segments underwent three gentle washes with PBS, followed by reimaging with IVIS to assess changes in fluorescence intensity before and after washing.

Intestinal retention of MLB

A total of 27 mice (female, 8 weeks old) were randomly assigned and orally administered with Cy5-NHS ester–labeled LA, MLB, and MLB@CA (1.0×10^8 CFUs). The GI tissue was removed and imaged using an IVIS at 2, 12, and 24 hours. Besides, the in vivo retention after a single dose was explored. Another batch of 27 mice was also evenly divided into three groups and orally administered with LA, MLB, and MLB@CA (1.0×10^8 CFUs). The GI tissues including the stomach, small intestine, cecum, and colon were harvested at 4, 48, and 96 hours post-oral gavage, homogenized, and diluted with PBS. Subsequently, the diluent (50 μl) was transferred to *Lactobacilli* selective agar plates for colony counting.

Preparation of MLB + IPA@CA microparticles

The method for preparing MLB + IPA@CA is essentially identical to that for preparing MLB@CA, except for adding IPA (1.5 mg/ml) to the solution.

EE and DLR of IPA

The freeze-dried MLB + IPA@CA (20 mg) was transferred to a sodium citrate solution (0.06 M, 5 ml) and gently shaken at 37°C until the microparticles were fully degraded. After centrifugation, 200 μl of the supernatant was retrieved and appropriately diluted for measuring IPA absorbance at 273 nm. The absorbance standard curve was constructed on the basis of known concentrations of IPA. The EE and DLR of IPA were calculated using the following formulas

$$\mathrm{EE} = \left(W_{\text{encapsulated IPA}} / W_{\text{total IPA}}\right) \times 100$$

$$\mathrm{DLR} = \left(W_{\text{encapsulated IPA}} / W_{\text{microparticles}}\right) \times 100$$

In vitro release characteristics of IPA

For the purpose of simulating the release profile of MLB + IPA@CA microparticles in the GI tract, 20 mg of freeze-dried MLB + IPA@CA were immersed separately in 2 ml of SGF and SIF with gentle shaking for 10 hours (37°C, 100 rpm). At specified time points, 200 μl of the supernatant was retrieved for absorbance measurement and supplemented with 200 μl of fresh buffer. The cumulative release concentration of IPA was calculated by summing up each release amount, which was calculated by measuring the absorbance at 273 nm.

Impact of IPA on LA viability

LA (1.0×10^8 CFUs) was coincubated with sterile PBS and IPA solution (1.5 mg/ml) for 4 hours, respectively. After centrifugation, bacterial pellets were collected for subsequent assay. For growth activity testing, the pellets were resuspended in MRS liquid medium and diluted to an initial OD_{600} of 0.1. Growth curves were generated by measuring OD_{600} at specified intervals. For colony counting, the pellets washed with PBS were resuspended in MRS liquid medium, and 50 μl of bacterial suspension was plated on MRS agar plates. For CCK-8 assay, the pellets were resuspended to an OD_{600} of 0.3, and, then, 10 μl of CCK-8 was introduced into 190 μl of the bacterial suspension. The OD_{450} of the bacterial suspension was measured hourly during incubation at 37°C.

Cytocompatibility assessment

The leachate of montmorillonite + IPA@CA microparticles was coincubated with NIH 3T3 cells for 1 to 3 days, with cells cultured in normal 3T3 cell medium as the control group. The cells were stained using the Calcein-AM/propidium iodide–staining method and observed under an inverted fluorescence microscope (MShot) to assess cell condition. In addition, cell proliferation was evaluated using the CCK-8 assay.

Biosafety assessment

To evaluate the in vivo safety of MLB + IPA@CA, BALB/c mice (female, 8 weeks old) were orally administered with the microparticles [containing 1.0×10^8 CFUs LA and IPA 20 mg/kg)] once daily for 5 days. Mice receiving 1.0% (w/v) CMC served as controls. The body weight was monitored daily throughout the study. On the 5th day, blood samples were collected to evaluate blood routine indices, liver function indices, and kidney function indices. Colon lengths were measured after removal. Major organs were collected for H&E staining.

Modeling and treatment of mice with colitis

Mice were randomly assigned, and all groups except for the healthy one were fed with drinking water containing 3.0% DSS for 7 days to induce colitis. The healthy group received CMC (1.0% w/v) treatment, while the DSS-induced colitis groups were given CMC, CA, LA (1.0×10^8 CFUs), MLB (1.0×10^8 CFUs LA), MLB@CA (1.0×10^8 CFUs LA), or MLB + IPA@CA (1.0×10^8 CFUs LA and 20 mg/kg IPA) by oral gavage once daily for 5 days. Disease progression was monitored by assessing body weight changes and DAI. On the final day, 100 mg of fecal samples were taken from each mouse for subsequent 16*S* rDNA sequencing and microbiota analysis. Blood samples were collected for ELISA quantification of inflammatory cytokines. Colon tissues were collected and promptly fixed for subsequent sectioning and staining.

ELISA analysis

The whole blood was centrifuged to collect the serum samples, which were then quantitatively analyzed for inflammatory cytokine concentrations using an ELISA kit (Thermo Fisher Scientific).

Histopathological analysis

Colon slices were H&E-stained following the manufacturer's protocol. Then, the slices were observed under an optical microscope to assess tissue morphology and infiltration of inflammatory cells.

MPO immunohistochemical staining

To assess MPO expression levels, antigen retrieval was performed on the colon slices, followed by incubation with a primary anti-MPO antibody and a secondary antibody conjugated with horseradish peroxidase. Visualization was achieved using 3,3′-diaminobenzidine (Servicebio).

Assessment of intestinal barrier function

Colon slices were stained with AB-PAS according to the manual instruction. The distribution of mucus and glycoprotein in colon tissue was observed under an optical microscope. For evaluation of physical barrier function, colon slices were incubated with primary antibodies against ZO-1 and Occludin-1, followed by appropriate secondary antibodies as directed by the manufacturer's guidelines. The distribution of both tight junction proteins was observed using fluorescence microscopy.

16*S* rDNA sequencing and microbiota analysis

Total DNA was extracted from microbial cells in fecal samples following cell lysis. A 16*S* rDNA library targeting the V4 hypervariable

region of bacterial 16*S* rDNA genes was constructed, and sequencing was conducted on the basis of the Illumina NovaSeq platform (Novogene). Data analysis was then conducted.

Statistical analysis

Data are presented as means ± SD. Significance was evaluated using Student's *t* test or one-way analysis of variance (ANOVA), with *P* value considered significant at < 0.05 ($^{*}P < 0.05$, $^{**}P < 0.01$, $^{***}P < 0.001$).

Supplementary Materials

This PDF file includes:

Figs. S1 to S17

REFERENCES AND NOTES

1. J. Zhou, M. Li, Q. Chen, X. Li, L. Chen, Z. Dong, W. Zhu, Y. Yang, Z. Liu, Q. Chen, Programmable probiotics modulate inflammation and gut microbiota for inflammatory bowel disease treatment after effective oral delivery. *Nat. Commun.* **13**, 3432 (2022).
2. S. Lin, S. Mukherjee, J. Li, W. Hou, C. Pan, J. Liu, Mucosal immunity–mediated modulation of the gut microbiome by oral delivery of probiotics into Peyer's patches. *Sci. Adv.* **7**, eabf0677 (2021).
3. X. Li, H. Sun, B. Li, X. Zhang, J. Cui, J. Yun, Y. Yang, L. e. Zhang, Q. Meng, S. Wu, J. Duan, H. Yang, J. Wu, Z. Sun, Y. Zou, R. Chen, Probiotics ameliorate colon epithelial injury induced by ambient ultrafine particles exposure. *Adv. Sci.* **6**, 1900972 (2019).
4. X. Yang, C. Wang, Q. Wang, Z. Zhang, W. Nie, L. Shang, Armored probiotics for oral delivery. *Smart Med.* **2**, e20230019 (2023).
5. Y. Yin, Z. Li, H. Gao, D. Zhou, Z. Zhu, L. Tao, W. Guan, Y. Gao, Y. Song, M. Wang, Microfluidics-derived microparticles with prebiotics and probiotics for enhanced in situ colonization and immunoregulation of colitis. *Nano Lett.* **24**, 1081–1089 (2024).
6. A. M. Vargason, S. Santhosh, A. C. Anselmo, Surface modifications for improved delivery and function of therapeutic bacteria. *Small* **16**, 2001705 (2020).
7. J. Yang, G. Zhang, X. Yang, M. Peng, S. Ge, S. Tan, Z. Wen, Y. Wang, S. Wu, Y. Liang, J. An, K. Zhang, J. Liu, J. Shi, Z. Zhang, An oral "Super probiotics" with versatile self-assembly adventitia for enhanced intestinal colonization by autonomous regulating the pathological microenvironment. *Chem. Eng. J.* **446**, 137204 (2022).
8. K. Zhang, L. Zhu, Y. Zhong, L. Xu, C. Lang, J. Chen, F. Yan, J. Li, J. Qiu, Y. Chen, D. Sun, G. Wang, K. Qu, X. Qin, W. Wu, Prodrug integrated envelope on probiotics to enhance target therapy for ulcerative colitis. *Adv. Sci.* **10**, 2205422 (2022).
9. Z. Li, A. M. Behrens, N. Ginat, S. Y. Tzeng, X. Lu, S. Sivan, R. Langer, A. Jaklenec, Biofilm-inspired encapsulation of probiotics for the treatment of complex infections. *Adv. Mater.* **30**, 1803925 (2018).
10. M. E. Sanders, D. J. Merenstein, G. Reid, G. R. Gibson, R. A. Rastall, Probiotics and prebiotics in intestinal health and disease: From biology to the clinic. *Nat. Rev. Gastroenterol. Hepatol.* **16**, 605–616 (2019).
11. C. Han, J. Song, J. Hu, H. Fu, Y. Feng, R. Mu, Z. Xing, Z. Wang, L. Wang, J. Zhang, C. Wang, L. Dong, Montmorillonite promotes probiotic biofilm formation in the gut for cancer immunotherapy. *Cell Rep.* **34**, 108706 (2021).
12. L. Shang, Y. Cheng, Y. Zhao, Emerging droplet microfluidics. *Chem. Rev.* **117**, 7964–8040 (2017).
13. C. Shao, J. Chi, L. Shang, Q. Fan, F. Ye, Droplet microfluidics-based biomedical microcarriers. *Acta Biomater.* **138**, 21–33 (2022).
14. L. Mei, F. He, R.-Q. Zhou, C.-D. Wu, R. Liang, R. Xie, X.-J. Ju, W. Wang, L.-Y. Chu, Novel intestinal-targeted Ca-alginate-based carrier for pH-responsive protection and release of lactic acid bacteria. *ACS Appl. Mater. Interfaces* **6**, 5962–5970 (2014).
15. R. Luo, J. Liu, Q. Cheng, M. Shionoya, C. Gao, R. Wang, Oral microsphere formulation of M2 macrophage-mimetic Janus nanomotor for targeted therapy of ulcerative colitis. *Sci. Adv.* **10**, eado6798 (2024).
16. X. Yang, W. Nie, C. Wang, Z. Fang, L. Shang, Microfluidic-based multifunctional microspheres for enhanced oral co-delivery of probiotics and postbiotics. *Biomaterials* **308**, 122564 (2024).
17. K. Yang, X. Wang, R. Huang, H. Wang, P. Lan, Y. Zhao, Prebiotics and postbiotics synergistic delivery microcapsules from microfluidics for treating colitis. *Adv. Sci.* **9**, 2104089 (2022).
18. C. Zhao, Y. Zhu, B. Kong, Y. Huang, D. Yan, H. Tan, L. Shang, Dual-core prebiotic microcapsule encapsulating probiotics for metabolic syndrome. *ACS Appl. Mater. Interfaces* **12**, 42586–42594 (2020).
19. T. Ramdhan, S. H. Ching, S. Prakash, B. Bhandari, Physical and mechanical properties of alginate based composite gels. *Trends Food Sci. Technol.* **106**, 150–159 (2020).
20. Y. Chen, S. Lin, L. Wang, Y. Zhang, H. Chen, Z. Fu, M. Zhang, H. Luo, J. Liu, Reinforcement of the intestinal mucosal barrier via mucus-penetrating PEGylated bacteria. *Nat. Biomed. Eng.* **8**, 823–841 (2024).
21. G. Lin, F. Yu, D. Li, Y. Chen, M. Zhang, K. Lu, N. Wang, S. Hu, Y. Zhao, H. Xu, Polydopamine-cladded montmorillonite micro-sheets as therapeutic platform repair the gut mucosal barrier of murine colitis through inhibiting oxidative stress. *Mater. Today Bio.* **20**, 100654 (2023).
22. J. Lloyd-Price, C. Arze, A. N. Ananthakrishnan, M. Schirmer, J. Avila-Pacheco, T. W. Poon, E. Andrews, N. J. Ajami, K. S. Bonham, C. J. Brislawn, D. Casero, H. Courtney, A. Gonzalez, T. G. Graeber, A. B. Hall, K. Lake, C. J. Landers, H. Mallick, D. R. Plichta, M. Prasad, G. Rahnavard, J. Sauk, D. Shungin, Y. Vázquez-Baeza, R. A. White, J. Braun, L. A. Denson, J. K. Jansson, R. Knight, S. Kugathasan, D. P. B. McGovern, J. F. Petrosino, T. S. Stappenbeck, H. S. Winter, C. B. Clish, E. A. Franzosa, H. Vlamakis, R. J. Xavier, C. Huttenhower, Multi-omics of the gut microbial ecosystem in inflammatory bowel diseases. *Nature* **569**, 655–662 (2019).
23. E. Elinav, T. Strowig, A. L. Kau, J. Henao-Mejia, C. A. Thaiss, C. J. Booth, D. R. Peaper, J. Bertin, S. C. Eisenbarth, J. I. Gordon, R. A. Flavell, NLRP6 inflammasome regulates colonic microbial ecology and risk for colitis. *Cell* **145**, 745–757 (2011).
24. J. Yu, J. Zhao, H. Xie, M. Cai, L. Yao, J. Li, L. Han, W. Chen, N. Yu, D. Peng, Dendrobium huoshanense polysaccharides ameliorate ulcerative colitis by improving intestinal mucosal barrier and regulating gut microbiota. *J. Funct. Foods* **96**, 105231 (2022).
25. Q. Wang, K. Xu, X. Cai, C. Wang, Y. Cao, J. Xiao, Rosmarinic acid restores colonic mucus secretion in colitis mice by regulating gut microbiota-derived metabolites and the activation of inflammasomes. *J. Agric. Food Chem.* **71**, 4571–4585 (2023).
26. S. Khan, S. Waliullah, V. Godfrey, M. A. W. Khan, R. A. Ramachandran, B. L. Cantarel, C. Behrendt, L. Peng, L. V. Hooper, H. Zaki, Dietary simple sugars alter microbial ecology in the gut and promote colitis in mice. *Sci. Transl. Med.* **12**, eaay6218 (2020).
27. M. T. Sorbara, E. R. Littmann, E. Fontana, T. U. Moody, C. E. Kohout, M. Gjonbalaj, V. Eaton, R. Seok, I. M. Leiner, E. G. Pamer, Functional and genomic variation between human-derived isolates of *Lachnospiraceae* reveals inter- and intra-species diversity. *Cell Host Microbe* **28**, 134–146.e4 (2020).
28. X. Kang, C. Liu, Y. Ding, Y. Ni, F. Ji, H. C. H. Lau, L. Jiang, J. J. Sung, S. H. Wong, J. Yu, *Roseburia intestinalis* generated butyrate boosts anti-PD-1 efficacy in colorectal cancer by activating cytotoxic $CD8^{+}$ T cells. *Gut* **72**, 2112–2122 (2023).
29. X. Yang, J. Yang, Z. Ye, G. Zhang, W. Nie, H. Cheng, M. Peng, K. Zhang, J. Liu, Z. Zhang, J. Shi, Physiologically inspired mucin coated *Escherichia coli* Nissle 1917 enhances biotherapy by regulating the pathological microenvironment to improve intestinal colonization. *ACS Nano* **16**, 4041–4058 (2022).
30. Z. Cao, S. Cheng, X. Wang, Y. Pang, J. Liu, Camouflaging bacteria by wrapping with cell membranes. *Nat. Commun.* **10**, 3452 (2019).
31. D. Alp, H. Kuleaşan, A. K. Altıntaş, The importance of the S-layer on the adhesion and aggregation ability of Lactic acid bacteria. *Mol. Biol. Rep.* **47**, 3449–3457 (2020).

Acknowledgments

Funding: This work was supported by the National Key Research and Development Program of China (2020YFA0908200), the National Natural Science Foundation of China (grant no. 32271383), and Core Facility of Shanghai Medical College, Fudan University. **Author contributions:** Conceptualization: L.S. and Z.F. Methodology: Z.F., X.Y., and L.S. Investigation: Z.F., X.Y., and L.S. Visualization: Z.F., X.Y. Writing—original draft: Z.F. Writing—review and editing: Z.F., X.Y., and L.S. Resources: L.S. Funding acquisition: L.S. Data curation: Z.F. and X.Y. Supervision: L.S. Formal analysis: Z.F. and X.Y. Project administration: L.S. **Competing interests:** The authors declare that they have no competing interests. **Data and materials availability:** All data needed to evaluate the conclusions in the paper are present in the paper and/or the Supplementary Materials.

Submitted 18 September 2024
Accepted 11 February 2025
Published 19 March 2025
10.1126/sciadv.adt2131